King's Research Portal

Link to publication record in King's Research Portal

The Bonding Nature Between Noble Gases and Small Gold Clusters

Piero Ferrari,[*,a] Laia Delgado-Callico,[b] Olga V. Lushchikova,[c] Matias Bejide,[a] Frank J. Wensink,[c] Joost M. Bakker,[c] Francesca Baletto,[b,d] and Ewald Janssens[*,a]
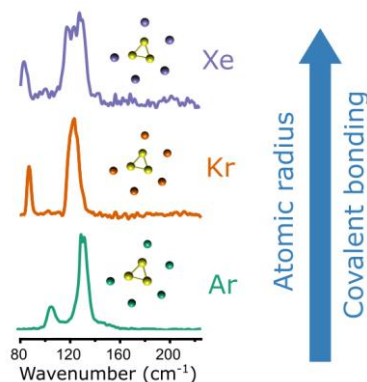
[a] Quantum Solid-State Physics, KU Leuven, Celestijnenlaan 200d, 3001 Leuven, Belgium

[b] Department of Physics, King's College London, London WC2R 2LS, UK

[c] Institute for Molecules and Materials, FELIX Laboratory, Radboud University, 6525 ED Nijmegen, Netherlands

[d] Department of Physics, University of Milan, Via Celoria 16, I-20133 Milano, Italy

TOC Graphic

ABSTRACT: Noble gases are usually seen as utterly inert, likewise gold, which is typically conceived as the noblest of all metals. While one may expect that noble gases bind to gold via dispersion interactions only, strong bonds can be formed between noble gas atoms and small gold clusters. We combine mass spectrometry, infrared spectroscopy, and density functional theory calculations to address the bonding nature between Au_n^+ ($n \leq 4$) clusters and Ar, Kr, and Xe. We unambiguously determine the geometries and quantitatively uncover the bonding nature in $Au_nNg_m^+$ (Ng = Ar, Kr, Xe) complexes. Each Au cluster can form covalent bonds with atop bound noble gas atoms, with strengths that increase with the noble gas atomic radius. This is demonstrated by calculated adsorption energies, Bader electron charges, and analysis of the electron density. The covalent bonding character, however, is limited to the atop coordinated Ng atoms.

According to the octet rule, the inertness of a noble gas (Ng) atom arises from its electronic configuration with fully occupied outermost s and p shells (except for He). The octet rule simultaneously rationalizes the stability of compounds such as CO_2, NaCl and MgO, which adopt the same electronic configuration to gain stability. The noble gas inertness is exploited in optical spectroscopy by messenger techniques [1], matrix isolation of reactive species [2], or solvation in He nanodroplets [3]. In mass-spectrometry, noble gas atoms are used as thermalization agents in laser ablation [4] and ion trapping via collisional cooling [5]. Recent developments in surface science use noble gas physisorption as a probe to monitor the photocatalytic activity of transition metal oxide surfaces [6], or to deposit catalytically active nanoparticles [7].

A noble gas atom can typically form weak bonds with other atoms or molecules via dispersion forces, but there are cases where strong bonds between a noble gas and certain metal ions or small clusters are formed [8, 9, 10, 11]. In 1995, Pyykkö proposed that the Au^+–Ng (Ng = Ar, Kr, Xe) bond had a partial covalent character [12], a claim that triggered discussions that persist until today [13, 14, 15, 16]. This idea is controversial, given the proverbial inertness of gold [17]. Currently, noble gas chemistry is a very

active research field [18, 19], central in understanding the bonding nature between noble gases and ions, molecules, and small clusters [20, 21, 22].

Gold has played a crucial role in the development of noble gas chemistry. As a heavy atom, gold has strong relativistic effects, which, e.g., provide a large electron affinity [23]. In comparison to Ag and Cu, Au^+-Ng complexes exhibit a larger electron transfer from Ng to Au and thus, a strong Au–Ng bond. The bond strength is also observed to increase with the size of the Ng atom. CCSD(T) calculations predict Au^+–Ng binding energies of 0.09, 0.15, 0.46, 0.71 and 1.16 eV, for Ng = He, Ne, Ar, Kr and Xe, respectively [12]. The high binding energies for Ar, Kr and Xe suggest chemical bonds with a partly covalent character. Nevertheless, the binding energy might also be attributed to higher Van der Waals interactions, given the increasing polarizability with Ng atomic radius [24].

Some experimental studies have suggested covalent interactions between noble gases and certain ions and small cluster species, particularly when Au is involved. Using $Au_3Ar_3^+$ as model system, Fielicke and co-workers combined infrared spectroscopy and density functional theory (DFT) calculations to show a prominent influence of Ar on

the vibrational modes of the metal-metal bonds, and attributed this to the formation of a partly covalent argon-gold bond [25]. Remarkably, the interaction weakens upon Ag doping, an analysis that was later extended to tetramers and pentamers [26].

To unambiguously differentiate the binding nature of Au with Ng atoms, we spectroscopically characterize small gold clusters with a variable number of Ng atoms. The combination of mass spectrometry and mass-selective infrared multiple photon dissociation (IRMPD) spectroscopy, complemented with high-level DFT calculations allows for an unambiguous assignment of the geometric structure of the cluster-Ng complexes, and a detailed insight into how the bonding nature changes when varying either the number of Ng atoms or the Ng atom specie.

These constitute the first experiments addressing the interaction of Au clusters with Ng atoms heavier than Ar [25], as well as the first where the number of Ng atoms exceeds that of Au atoms, so that each Ng atom can no longer coordinate to a single Au atom, without competitive co-adsorption of other Ng atoms. High-quality experimental information on the geometric structure of such complexes is fundamental for addressing the nature of the Au_n^+–Ng bond, which has only been discussed theoretically in ongoing debates on the exact covalent contribution [18, 24, 20]. It is, for example, unknown whether a single Au atom can form one or even multiple covalent bonds with Ar. Since the balance between dispersive and covalent interactions determines the chemistry of these Ng complexes, a thorough understanding of their bonding nature is crucial for the design of novel chemical compounds involving such species.

Gold cluster-Ng complexes are formed by pulsed laser ablation and gas condensation [27], in a cluster source kept at 200 K, using as carrier gas a mixture of 2% of Ng in He. The cluster-carrier gas mixture expands into vacuum through a conical nozzle, after which the formed cluster beam is collimated before entering a perpendicularly extracted time-of-flight mass spectrometer (see the supporting information (SI) for details). The experimentally formed mass distributions of $Au_nNg_m^+$ clusters, per Ng species, are characterized in Figure 1 by the complexation branching ratio $F_{nm}(Ng)$

$$F_{nm}(Ng) = \frac{I_{nm}(Ng)}{\sum_{i=0}^{6} I_{ni}(Ng)}, \qquad (1)$$

with $I_{nm}(Ng)$ the spectral mass abundance of $Au_nNg_m^+$, and i running for the number of Ng atoms attached per Au_n^+. Under the employed experimental conditions, up to 6 Ng atoms are attached per cluster. Figure 1 shows that: 1) complexation of Au_n^+ with Kr and Xe is easier than for Ar, suggesting a stronger bond formation for these Ng atoms, and 2) Au_3^+ and Au_4^+ clusters preferentially bind 3 and 4 Kr or Xe atoms, respectively, suggesting the formation of stronger Au-Ng bonds if $m \leq n$ than if $m > n$.
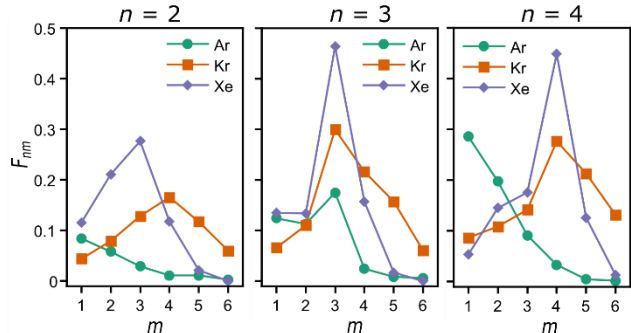

Figure 1. Complexation branching ratios of noble gas complexes of Au_n^+ (n = 2–4) for Ng = Ar, Kr and Xe, in mass spectra recorded under similar experimental conditions.

The experimental infrared spectra of $Au_nNg_m^+$ (n = 2–4; Ng = Ar, Kr, Xe) are shown in the top of each panel in Figure 2. To record IRMPD spectra, the formed cluster beam is overlapped with the laser light of the free electron laser FELICE, with the particular feature that the cluster-light interaction occurs within the laser cavity [28]. Upon resonant photon absorption, Ng atoms desorb from the $Au_nNg_m^+$ complexes, allowing the construction of depletion spectra as a function of the excitation wavelength, which then are converted into IRMPD spectra. For each Au_n^+ cluster (each column in Figure 2), the infrared spectra presented are those for complexes with the same number of Ng atoms (the same m, all in one column), where m is chosen such that each $Au_nNg_m^+$ only shows depletion upon resonant photon absorption [29]. For example, the Ng loss channel of $Au_3Ng_5^+$ ($Au_3Ng_5^+ + x \cdot h\nu \rightarrow Au_3Ng_4^+ + Ng$, with x an unknown number of photons at frequency ν) affects the signal of $Au_3Ng_4^+$, which may not just show depletion but also gain. Therefore, although $Au_3Ng_3^+$ is the most prominent peak in mass spectra for n = 3, the analysis of infrared spectra is performed for $Au_3Ng_5^+$, which is the $Au_3Ng_m^+$ complex with the lowest number of attached Ng atoms showing depletion only. The high signal-to-noise ratio of the recorded spectra allows for an unambiguous assignment to specific geometries. The DFT-calculated vibrational spectra of the lowest-energy isomers for each cluster size are shown in Figure 2, with the cross section σ constructed by assuming Gaussian functions around each calculated frequency, with a full width at half maximum of 5 cm⁻¹. The calculations are performed using the ORCA 4.2.1 software package [30], employing the PBE functional in combination with dispersion corrections (D3BJ) and the Def2-QZVPP basis set. The Def2 effective core potentials (ECPs) from Ahlrichs were employed for Au and Xe, whereas all the electrons of Ar and Kr were included explicitly. This level of theory was selected based on two previous studies, where a correct description of Ng interactions with gold clusters was shown [21, 29]. While for $Au_2Ng_4^+$ and $Au_3Ng_5^+$ only one isomer is found for the Au_2^+ and Au_3^+ frameworks, a second Au_4^+ isomer in $Au_4Ng_4^+$ is presented in the SI. Moreover, for $Au_3Ng_5^+$, a second stable configuration of the Ng atoms is shown in the SI. Importantly, this additional configuration also has three Ng atoms adsorbed on an atop coordination. The geometries

assigned for the metallic frameworks in the complexed clusters are the same as those determined for the bare clusters [29, 31], implying that complexation with Kr and Xe does not affect the geometry of the underlying metal framework. Hence, the differences in the spectra of $Au_nNg_m^+$ for different Ng (but identical n, m), can provide information on the Au_n^+-Ng_m bonding strength [25].
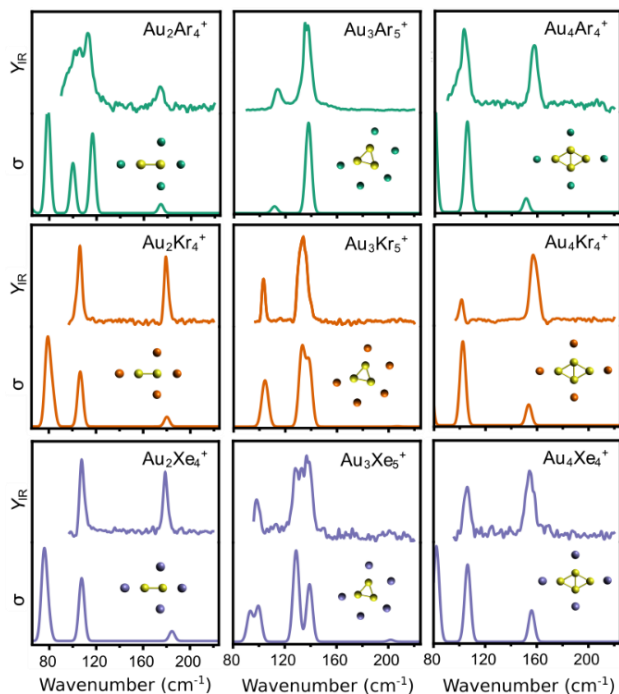

Figure 2. Experimental (top of each panel) and calculated (bottom) infrared spectra of $Au_2Ng_4^+$ (left), $Au_3Ng_5^+$ (middle) and $Au_4Ng_4^+$ (right). Each cluster's geometry appears as an inset, with Au (yellow), Ar (green), Kr (orange) and Xe (purple).

The spectrum for $Au_2Ar_4^+$ (first panel of Figure 2; top-left) reveals three infrared active modes (two partly overlapped) in the recorded spectral range, while the spectra for $Au_2Kr_4^+$ and $Au_2Xe_4^+$ only show two. The calculations for $Au_2Ar_4^+$ predict the high-frequency band at 174 cm⁻¹, and identify it as the symmetric combination of the two Au–Ar stretches (with the two Ar on the Au–Au axis). This mode is also present for $Au_2Kr_4^+$ and $Au_2Xe_4^+$, although at slightly higher frequencies (180 and 185 cm⁻¹). This symmetric mode is not expected to be infrared active, but it gains intensity due to the symmetry breaking caused by the two off-axis Ar atoms (calculations on $Au_2Ng_2^+$ show an IR-forbidden transition). An isomer with these off-axis Ar atoms in symmetric positions only show one vibrational mode in the measured spectral range (around 120 cm⁻¹) and can therefore be discarded. The experimental bands of $Au_2Ar_4^+$ at 103 and 112 cm⁻¹ (frequencies based on a fitting with two Gaussian functions) correspond to the breathing mode and the antisymmetric combination of the two Au–Ar stretches mentioned above. For $Au_2Kr_4^+$ and $Au_2Xe_4^+$, calculations predict that the breathing mode and the antisymmetric stretch combination are near-degenerate,

agreeing with the experiments by only showing a single band below 120 cm⁻¹. The spectra for Au_4^+ with four Ng atoms (Figure 2, right column) have two pronounced bands, corresponding to the antisymmetric combinations of the Au—Ng stretches along the short and long axes of the rhombic Au_4^+, respectively. For these modes no clear Ng dependence is found.
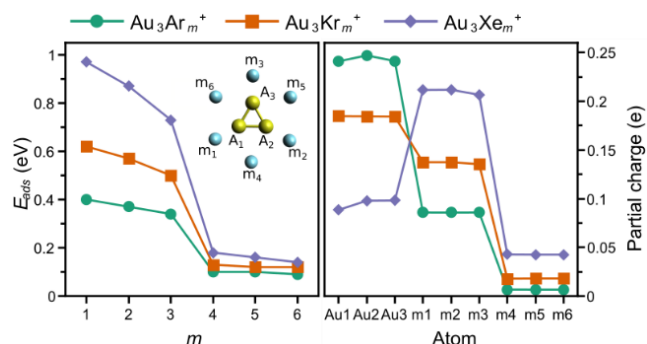

Figure 3. (Left) Adsorption energies of the m-th attached Ng atom in the $Au_3Ng_m^+$ cluster. (Right) Partial Bader charge on each atom in the $Au_3Ng_6^+$ cluster. Ar is shown in green, Kr in red, and Xe in blue.

The Ng-dependent variation in vibrational band positions is most pronounced in the IR spectra of $Au_3Ng_5^+$ (Figure 2, middle column). The spectrum of $Au_3Ar_5^+$ has two bands at 115 and 137 cm⁻¹ and is very different from the calculated spectrum of Au_3^+ (see SI). The DFT calculations reveal that each band is composed of two near-degenerate combinations of Au—Ar stretch vibrations, involving the atop coordinated Ar atoms. The Ar atoms on bridge sites, instead, barely participate in these vibrational modes (the corresponding atom displacements are shown in the SI). The most intense $Au_3Kr_5^+$ band is broader in the experiment, which can be attributed to a slight splitting of the two near-degenerate 137 cm⁻¹ modes of $Au_3Ar_5^+$, now found at 133 and 138 cm⁻¹. The degeneracy lifting is even stronger in $Au_3Xe_5^+$, with the experiment showing a significant broadening around 130 cm⁻¹, likely harboring more than one mode, which the calculations predict at 129 and 139 cm⁻¹. A calculation of $Au_3Ng_6^+$ reveals that indeed the cluster symmetry and degeneracies are restored, suggesting it is the involvement of the bridge-coordinated Xe atoms that break the symmetry of the complex. Interestingly, all the geometries of the complexes in Figure 2 are found to be planar, despite the large number of Ng atoms attached.

Overall, the mass spectra in Figure 1 with the shifting of bands observed in both experimental and calculated spectra for the $Au_3Ng_5^+$ complexes (Figure 2) suggest that the strength of the cluster-noble gas interaction follows the sequence Ar < Kr < Xe. Both the energetics and the electronic structure of the $Au_3Ng_6^+$ complexes confirm this hypothesis. The calculated adsorption energies E_{ads} of the mth attached Ng atom in $Au_3Ng_m^+$ [$E_{ads}=E(Au_3Ng_m^+)-E(Au_3Ng_{m-1}^+)-E(Ng)$; E the total energy] are shown in Figure 3 (left), with their magnitudes following the sequence Ar < Kr < Xe, consistent with the experiments. The counterpoise method

was used to quantify possible basis set superposition errors, showing an insignificant effect. For each Ng the first three Ng atoms bind strongly, with E_{ads} values around 0.4, 0.6 and 0.9 eV for Ar, Kr and Xe, respectively. Such high values are consistent with the formation of a partially covalent bond between Au and the atop attached Ng atoms. These first three Ng atoms actively participate in the vibrational modes seen in Figure 2. For $m = 4$-6, adsorption energies are much smaller (< 0.2 eV), but still follow the order Ar < Kr < Xe.

The partial Bader charges for $Au_3Ng_6^+$ are presented in Figure 3 (right). The Ng to Au electron donation is very pronounced for the first three, atop coordinated, Ng atoms, whereas charge donation from the bridge-coordinated Ng atoms ($m = 4$-6) is much smaller. Moreover, the charge transfer increases from Ar to Xe, both for atop-coordinated and bridge-bound Ng atoms. The charge transfer for Xe is so pronounced that the three atop-coordinated Xe atoms have higher partial positive charges than the Au atoms. The same conclusions are obtained from an analysis of Löwdin partial charges, in which the Ng to Au electron charge donations are even more pronounced (see SI for details). We conclude that the adsorption energy and the partial charge are correlated, with stronger Ng to Au electron transfers corresponding to higher adsorption energies. The lower adsorption energies and smaller charge transfers for the bridging Ng atoms suggest bonds with much smaller, if any, covalent character. To complement these observations, in the SI similar calculations for the neutral Au_3Ng_5 and the silver-based $Ag_3Ng_5^+$ complexes are presented. In the former, only one of the Au atoms accepts some electron transfer from a Ng. In particular, three of the Ng atoms have essentially zero partial charge, showing a weak bond that is reflected in the loose adsorption sites they adopt. For $Ag_3Ng_5^+$, results are similar to those of $Au_3Ng_5^+$, but with lower electron charge transfers.
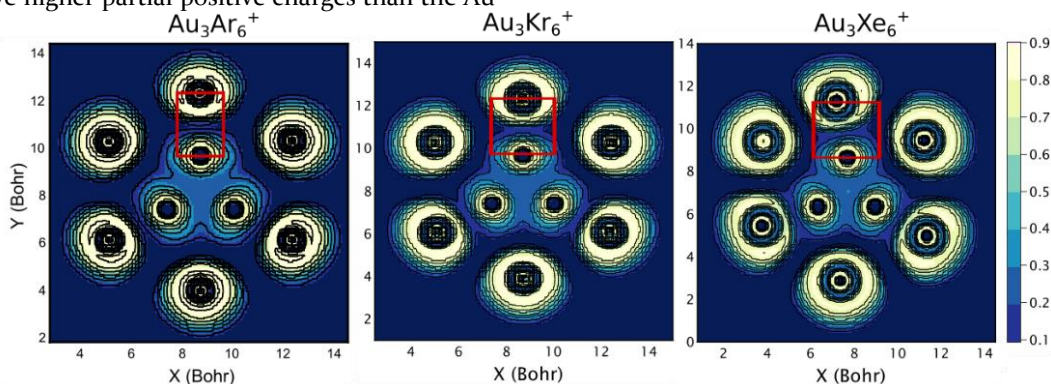

Figure 4. Contour plot of the Electron Localization Function (ELF) in the clusters $Au_3Ar_6^+$ (left), $Au_3Kr_6^+$ (middle) and $Au_3Xe_6^+$ (right). Colour code represents ELF values in the plane formed by the atoms. The red rectangles highlight the regions where the ELF plots are very different between the three Ng complexes.

The bonding between Au and the different Ng atoms in $Au_3Ng_6^+$ is visualized using the Electron Localization Function (ELF) in Figure 4, which represents the probability of finding an electron in the vicinity of another, reference, electron. For physical bonds, ELF values below 0.1 between atoms have been reported [32]. High ELF values are seen around Au_3 (~0.250), reflecting the pronounced covalent character of the Au-Au bonds. For $Au_3Ar_6^+$, the ELF values at the bond critical point (BCP) between Au and atop Ar atoms are lower, but not zero (0.127). Conversely, much lower ELF values are found at the BCP in between Au and the bridge-coordinated Ar atoms (~0.023). These results align with a partial covalent bond formation between Au and Ar atoms adsorbed in atop positions. The ELF analysis shows that the covalent character of the bond formed by Au and the atop adsorbed Ng atoms increase for Kr (0.179) and Xe (0.263). For the bridge-coordinated Ng atoms, ELF values are also smaller for Kr (0.031) and Xe (0.033). Plots of partial density of states are presented in the SI and are in agreement with the analysis presented here.

A topological analysis of the clusters was conducted based on the electron (ρ_{BCP}) and energy (H_{BCP}) densities at the BCPs. A covalent bond is characterized by ρ_{BCP} values in the $\approx 10^{-1}$ a.u. range, while for dispersive bonds these are lower ($\approx 10^{-2}$ a.u.) [33]. Furthermore, covalent bonds are characterized by negative H_{BCP} values, opposite to the positive H_{BCP} results for physical bonds. In Table 1, values of ρ_{BCP} and H_{BCP} at the BCPs, as well as the ELF values, are presented. Clearly, the topological analysis is consistent with a partly covalent bond between Au and the atop coordinated Ng atoms, with an increasing covalent character for larger Ng atoms. In contrast, the analysis suggests that the bridge coordinated Ng atoms form a bond of a dispersive nature.

In addition, the Au—Ng bonding is characterised with Wiberg (W) indexes (Table 1), calculated between Au and the atop- and bridge-coordinated Ng atoms in $Au_3Ng_6^+$. Typically, bonds with W indexes exceeding 0.5 are characterized as covalent [34]. For the atop-coordinated Ng atoms, W values are high, all above 0.5, in agreement with bonds having significant covalent character. In contrast, the values of the bridge-coordinated Ng atoms are below 0.5. An Energy Decomposition Analysis (EDA) and a Natural Bond Orbital (NBO) analysis of the bonds between Au_3^+-Ng and $Au_3Ng_3^+$-Ng is presented in the SI. In both clusters, the partial covalent character of the bond formation between atop-coordinated Ng atoms and Au_3^+ is

evident, while it is not the case for bridge-coordinated Ng atoms.

Table 1. Values of electron density (ρ_{BCP}), energy density (H_{BCP}) and electron localization function (ELF_{BCP}) at the bond critical points (BCP), in addition to Wiberg indexes, for $Au_3Ng_6^+$ complexes. Values correspond to Ng atoms at atop or bridge coordinations. The values of ρ_{BCP} and H_{BCP} are given in a.u.

Complex		ρ_{BCP}	H_{BCP}	ELF_{BCP}	W
$Au_3Ar_6^+$	atop	0.045	-0.0051	0.127	0.91
	bridge	0.006	0.0009	0.023	0.13
$Au_3Kr_6^+$	atop	0.052	-0.0089	0.179	1.14
	bridge	0.007	0.0009	0.031	0.17
$Au_3Xe_6^+$	atop	0.058	-0.0139	0.263	1.39
	bridge	0.006	0.0008	0.033	0.22

In conclusion, our joint experimental and computational study provides solid and quantifiable evidence for the formation of covalent Au-Ng bonds in $Au_nNg_m^+$ complexes. The Ng atom binds to Au in an atop coordination site. The covalent character increases with Ng atomic radius. For bridge-coordinated Ng atoms, instead, the bond is predominantly dispersive in nature.

ASSOCIATED CONTENT

Supporting Information. Experimental and computational methods; Representative mass spectra of $Au_nNg_m^+$ clusters; Isomer of $Au_4Ng_4^+$; Ng isomers of $Au_3Ng_5^+$; Au-Au interatomic distances in Au_n^+ and $Au_nNg_m^+$; Calculated IR spectra of Au_3^+ and $Au_3Ng_5^+$; Calculated infrared spectra of $Au_2Ng_4^+$, $Au_3Ng_5^+$, $Au_4Ng_5^+$ in a larger spectral range; Visual representation of the vibrational modes of $Au_nNg_m^+$ complexes; Löwdin partial charges in Au_3Ng_5+; Electron localization function in $Au_3Ng_5^+$; Ng adsorption energies in $Au_2Ng_m^+$ and $Au_4Ng_m^+$; Geometries and Bader charges of Au_3Ng_5 and $Ag_3Ng_5^+$; Analysis of partial density of states; Energy decomposition analysis (EDA) of Au_3-Ng^+ and Au_3-Ng_4^+; Natural bonding orbital (NBO) analysis of Au_3Ng^+ and $Au_3Ng_4^+$; XYZ coordinates. This material is available free of charge via the Internet at http://pubs.acs.org.

AUTHOR INFORMATION

Corresponding Author

* piero.ferrari@kuleuven.be
* ewald.janssens@kuleuven.be

Author Contributions

PF, OL, MB and FW performed the experiments. PF and LDC conducted the calculations. PF, FB, JB and EJ secured funding. PF and EJ initiated and directed the research project. PF, LDC, JB and EJ prepared the first version of the manuscript. All authors discussed the results and participated in writing the manuscript.

ACKNOWLEDGMENT

REFERENCES

(1) Goldsmith, B. R.; Florian, J.; Liu, J.-X.; Gruene, P.; Lyon, J. T.; Rayner, D. M.; Fielicke, A.; Scheffler, M.; Ghiringhelli, L. M. Two-to-Three Dimensional Transition in Neutral Gold Clusters: The Crucial Role of van der Waals Interactions and Temperature. *Phys. Rev. Materials* **2019**, *3*, 016002.

(2) Lecoultre, S.; Rydlo, A.; Félix, C.; Buttet, J.; Gilb, S.; Harbich, W. UV–Visible Absorption of Small Gold Clusters in Neon: Aun (n = 1–5 and 7–9). *J. Chem. Phys.* **2011**, *134*, 074302.

(3) Albertini, S.; Martini, P.; Schiller, A.; Schöbel, H.; Ghavidel, E.; Ončák, M.; Echt, O.; Scheier, P. Electronic Transitions in Rb_2^+ Dimers Solvated in Helium. *Theor. Chem. Acc.* **2021**, *140*, 29.

(4) Ferrari, P.; Sanzone, G.; Yin, J.; Janssens, E. Physical Synthesis of Nanoalloys, in Nanoalloys, Elsevier, **2020**, pp. 1–31.

(5) Lang, S. M.; Bernhardt, T. M.; Barnett, R. N.; Landman, U. Temperature-Tunable Selective Methane Catalysis on Au_2^+: From Cryogenic Partial Oxidation Yielding Formaldehyde to Cold Ethylene Production. *J. Phys. Chem. C* **2011**, *115*, 6788–6795.

(6) Tamijani, A. A.; Salam, A.; de Lara-Castells, M. P. Adsorption of Noble-Gas Atoms on the $TiO_2(110)$ Surface: An Ab Initio-Assisted Study with van der Waals-Corrected DFT. *J. Phys. Chem. C* **2016**, *120*, 18126–18139.

(7) Wu, Q.; Ridge, C. J.; Zhao, S.; Zakharov, D.; Cen, J.; Tong, X.; Connors, E.; Su, D.; Stach, E. A.; Lindsay, C. M.; Orlov, A. A. Development of a New Generation of Stable, Tunable, and Catalytically Active Nanoparticles Produced by the Helium Nanodroplet Deposition Method. *J. Phys. Chem. Lett.* **2016**, *7*, 2910–2914.

(8) Saha, R.; Jana, G.; Pan, P.; Merino, G.; Chattaraj, P. K. How Far Can One Push the Noble Gases Towards Bonding? *Molecules* **2019**, *24*, 2933.

(9) Saha, R.; Pan, S.; Mandal, S.; Orozco, M.; Merino, G.; Chattaraj, P. K. Noble Gas Supported B_3^+ Cluster: Formation of Strong Covalent Noble Gas–Boron Bonds. *RSC Adv.* **2016**, *6*, 78611–78620.

(10) Grabowski, S. J.; Ugalde, J. M.; Andrada, D. M.; Frenking. G. Comparison of Hydrogen and Gold Bonding in $[XHX]^-$, $[XAuX]^-$, and Isoelectronic $[NgHNg]^+$, $[NgAuNg]^+$

(X=Halogen, Ng=Noble Gas). *Chem. Eur. J.* **2016**, *22*, 11317–11328.

(11) Mück, L. A.; Timoshkin, A. Y.; von Hopffgarten, M.; Frenking, G. Donor Acceptor Complexes of Noble Gases. *J. Am. Chem. Soc.* **2009**, *131*, 3942–3949.

(12) Pyykko, P. Predicted Chemical Bonds Between Rare Gases and Au+. *J. Am. Chem. Soc.* **1995**, *117*, 2067–2070.

(13) Read, J. P.; Buckingham, A. D. Covalency in ArAu+ and Related Species? *J. Am. Chem. Soc.* **1997**, *119*, 9010–9013.

(14) Bellert, D.; Breckenridge, W. H. Bonding in Ground-State and Excited-State A+·Rg van der Waals Ions (A = Atom, Rg = Rare-Gas Atom): A Model-Potential Analysis. *Chem. Rev.* **2002**, *102*, 1595–1622.

(15) Belpassi, L.; Infante, I.; Tarantelli, F.; Visscher, L. The Chemical Bond Between Au(I) and the Noble Gases. Comparative Study of NgAuF and NgAu+ (Ng = Ar, Kr, Xe) by Density Functional and Coupled Cluster Methods. *J. Am. Chem. Soc.* **2008**, *1303*, 1048–1060.

(16) Jamshidi, Z.; Lushchikova, O. V.; Bakker, J. M.; Visscher, L. Not Completely Innocent: How Argon Binding Perturbs Cationic Copper Clusters. *J. Phys. Chem. A* **2020**, *124*, 9004–9010.

(17) Hammer, B.; Norskov, J. K. Why Gold is the Noblest of all the Metals. *Nature* **1995**, *376*, 238–240.

(18) Pan, S.; Jana, G.; Merino, B.; Chattaraj, P. K. Noble-Noble Strong Union: Gold at its Best to Make a Bond With a Noble Gas Atom. *ChemistryOpen* **2019**, 8, 173-187.

(19) Grandinetti, F. Noble Gas Chemistry: Structure, Bonding, and Gas-Phase Chemistry, Germany: John Wiley & Sons, 2018.

(20) Ghosh, A.; Ghanty, T. K. Unprecedented Enhancement of Noble Gas–Noble Metal Bonding in NgAu3+ (Ng = Ar, Kr, and Xe) Ion through Hydrogen Doping. *J. Phys. Chem. A* **2016**, *120*, 9998–10006.

(21) Delgado-Callico, L.; Ferrari, P.; Bakker, J. M.; Baletto, F.; Janssens, E. Benchmarking Density Functional Theory Methods for Modelling Cationic Metal–Argon Complexes. *Theor. Chem. Acc.* **2021**, *140*, 38.

(22) Wöhner, K.; Wulf, T.; Vankova, N.; Heine, T. Strong Binding of Noble Gases to $[B_{12}X_{11}]^-$: A Theoretical Study. *J. Phys. Chem. A* **2021**, *125*, 4760–4765.

(23) Pyykko, P. Relativistic Effects in Structural Chemistry. *Chem. Rev.* **1988**, *88*, 563–594.

(24) Pan, P.; Saha, R.; Mandal, S.; Chattaraj, P. K. σ-Aromatic Cyclic M3+ (M = Cu, Ag, Au) Clusters and Their Complexation With Dimethyl Imidazol-2-ylidene, Pyridine, Isoxazole, Furan, Noble Gases and Carbon Monoxide. *Phys. Chem. Chem. Phys.* **2016**, *18*, 11661–11676.

(25) Shayeghi, A.; Johnston, R. L.; Rayner, D. M.; Schäfer, R.; Fielicke, A. The Nature of Bonding Between Argon and Mixed Gold–Silver Trimers. *Angew. Chem. Int. Ed.* **2015**, *54*, 10675–0680.

(26) Shayeghi, A.; Schäfer, R.; Rayner, D. M.; Johnston, R. L.; Fielicke, A. Charge-Induced Dipole vs. Relativistically Enhanced Covalent Interactions in Ar-Tagged Au-Ag Tetramers and Pentamers. *J. Chem. Phys.* **2015**, *143*, 024310.

(27) Duncan, M. A. Invited Review Article: Laser Vaporization Cluster Sources. *Rev. Sci. Instrum.* **2012**, *83*, 041101.

(28) Bakker, J. M.; Lapoutre, V. J. F.; Redlich, B.; Oomens, J.; Sartakov, B. G.; Fielicke, A.; von Helden, G.; Meijer, G.; van der Meer, A. F. G. Intensity-Resolved IR Multiple Photon Ionization and Fragmentation of C_{60} *J. Chem. Phys.* **2010**, *132*, 074305.

(29) Ferrari, P.; Hou, G.-L.; Lushchikova, O. L.; Calvo, F.; Bakker, J. M.; Janssens, E. The Structures of Cationic Gold Clusters Probed by Far-Infrared Spectroscopy. *Phys. Chem. Chem. Phys.* **2020**, *22*, 11572–11577.

(30) Neese, F.; Wennmohs, F.; Becker, U.; Riplinger, C. The ORCA Quantum Chemistry Program Package. *J. Chem. Phys.* **2020**, *152*, 224108.

(31) Gilb, S.; Weis, P.; Furche, F.; Ahlrichs, R.; Kappes, M. M. Structures of small gold cluster cations (Au_n+, n<14): Ion Mobility Measurements Versus Density Functional Calculations *J. Chem. Phys.* **2002**, *116*, 4094.

(32) Koumpouras, K.; Larsson, J. A. Distinguishing Between Chemical Bonding and Physical Binding Using Electron Localization Function (ELF). *J. Phys.: Condens. Matter.* **2020**, *32*, 315502.

(33) Barabás, J.; Vanbuel, J.; Ferrari, P.; Janssens, E.; Höltzl, T. Non-Covalent Interactions and Charge Transfer Between Propene and Neutral Yttrium-Doped and Pure Gold Clusters. *Chem. Eur. J.* **2019**. 25, 15795–15804.

(34) Arrué, L.; Pino-Rios, R. On the Stability and Chemical Bond of Noble Gas Halide Cations NgX+ (Ng = He – Rn; X = F – I). *J. Comput. Chem.* **2020**, *42*, 124-129.